Dual parton model for the charged multiplicity in $p-p$ collisions at 13, 13.6 TeV and for a future LHC energy of 27 TeV

Pranay K. Damuka[*] and R. Aggarwal[†]
Department of Technology, Savitribai Phule Pune University, Pune 411007, India

M. Kaur[‡]
Department of Physics, Panjab University, Chandigarh 160014, India
and Department of Physics, Amity University, Punjab, Mohali 140306, India

(Received 10 August 2022; accepted 10 October 2022; published 28 October 2022)

Analysis of the charged multiplicity in proton-proton inelastic interactions at the LHC energies in the setting of the dual parton model is presented. Data from the CMS experiment and the data simulated at different energies in various pseudorapidity windows using the event generator PYTHIA8 are analyzed and compared with the calculations from the model. Each inelastic scattering is assumed to follow the Poisson distribution. The Koba-Nielsen-Olesen (KNO) scaling of the multiplicity distributions is studied and compared with previously published experimental results at $\sqrt{s} = 0.9$, 2.36, 7 TeV. Predictions from the model for the KNO distributions at $\sqrt{s} = 13$, 13.6 TeV and for the future LHC energy of 27 TeV are computed and compared with the simulated data.

DOI: 10.1103/PhysRevD.106.076017

I. INTRODUCTION

The number of charged particles produced in a high-energy particle interaction gives a measure of an important quantity known as multiplicity. One can validate the predictions from a theoretical or phenomenological model by studying the multiplicity distribution (MD) of the charged particles obtained from the experimental observations. The study of charged particles production gives information about both the soft QCD processes and the hard interactions and of the transition between the two. The hard scattering part can be obtained from the theoretical perturbative calculations; however, the soft part is gauged by the nonperturbative phenomenological models.

Interest in MD was stimulated by a paper of Koba *et al.* [1] in 1972, in which they established a scaling behavior of the MD. They showed that the multiplicity follows a universal scaling behavior at high energies and termed it as the Koba-Nielsen-Olesen (KNO) scaling. The scaled distribution, with the parameters $z = n/\langle n\rangle$ and $\Psi(z) = \langle n\rangle P_n$, is independent of energy, where P_n is the probability of producing n charged hadrons with a mean value of $\langle n\rangle$. The very first KNO violation was observed at the CERN collider in $\bar{p}p$ collisions at $\sqrt{s} = 540$ GeV [2]. Soon after, the violation was also reported by different experiments involving particle interactions at other energies with different species of particles [3–6]. In the present work, analysis of the multiplicity distributions in pp interactions at the LHC energies is described in the framework of the dual parton model (DPM) [7–11]. The DPM was first introduced in 1979 by Capella *et al.* [7]. In 1982, the quark gluon string model (QGSM) was introduced by Kaidalov and Ter-Martirosyan, which is similar to the DPM with some essential differences [12,13]. Both DPM and QGSM are based on the Reggeon field theory (RFT) [14].

The use of DPM to describe the soft interactions started with a single Pomeron exchange. Later, multiple Pomeron exchange diagrams were included and referred to as multiple scattering DPM. The DPM makes use of the dual topological unitarization (DTU) scheme [15–19] to make unitarity cuts on the Pomeron exchange diagrams. In this model, a weight is associated with the cross section of each diagram appearing in the DTU expansion. The use of DPM to define the hadron multiplicity is described briefly in the Sec. II.

The DPM has been observed to not only describe the experimental charged particle multiplicities energies at the Intersecting Storage Rings (ISR) energies but could also account for scaling violation observed at the UA5

[*]pranaydamuka546@gmail.com
[†]ritu.aggarwal1@gmail.com
[‡]manjit@pu.ac.in

experiment [9,10]. The success of the DPM is limited not only to the hadron-hadron collisions, but it has been extended to the hadron-nucleus [20–23] and nucleus-nucleus [21,24,25] collisions as well. It is relevant to mention here the recent observations of ridgelike structure in the near side of the $\Delta\eta - \Delta\phi$ two-particle correlation distributions made by the CMS and ATLAS collaborations at the LHC [26–28]. This structure becomes more prominent for the high-multiplicity events. Such results are implicative for the nuclear collisions data and signaled the presence of strong collectivity in the nuclear collisions [29,30]. However, these were least expected for the small and short-lived pp systems. There have been some advancements in terms of explanations given to explain the near-ridge structure in different collisions systems. The hydrodynamical evolution [31] and formation of the color glass condensate [32,33] are possible explanations for this observation. In this study [34,35], the ridge structure was explained by the emission of the correlated clusters in the azimuthal phase space, and it was explained using string percolation model in another study [36,37].

The charged particle multiplicities data from the nonsingle diffractive (NSD) pp and AA collisions at the LHC energy of 2.76 TeV have also been found to follow the predictions for nondiffractive (ND) charged multiplicities calculated from the DPM [38,39]. The contribution from the double diffractive processes is small [40,41], which makes the NSD experimental data and ND calculations from the model comparable. The ability of the DPM to describe the hadronic spectra from high-energy collisions of particles of various species motivates us to study the pp collisions in the framework of the DPM. The LHC has started producing data for pp collisions at $\sqrt{s} = 13.6$ TeV, which is the highest energy that has been ever achieved. In this paper, the experimental charged particle multiplicities from the CMS Collaboration at $\sqrt{s} = 0.9$, 2.36, 7 TeV [42] are studied using the DPM in the form of KNO distributions, which are in agreement with the experimental data. The average charged multiplicities for these collisions are calculated using DPM and are compared to the experimental results. For each of the collision energies, simulated data are produced using PYTHIA8 and compared to the predictions from the DPM and to the results from the CMS experiment.

The main highlights of this paper are the predictions of the charged particle multiplicities, KNO distributions, and average multiplicities for the present LHC RUN3 energy of 13.6 TeV and the future LHC energy of 27 TeV in addition to the LHC RUN2 energy of 13 TeV using the DPM. These calculations are presented for the inelastic pp scatterings in two central pseudorapidity intervals of 0.5 and 2.4. Simulated data are produced for the NSD pp collisions at the energies of 13, 13.6, and 27 TeV in the two psuedorapidity intervals. A detailed comparison of the KNO distributions and average multiplicities is presented in this paper using DPM calculations and predictions from PYTHIA8.

II. MODEL

In the DPM, an inelastic scattering is considered as an exchange of a Pomeron between colliding hadrons, which results in two strings when a unitarity cut is made on the Pomeron. In a multiple scattering DPM, multiple Pomerons are exchanged, which gives rise to twice the number of strings when the DTU expansion scheme is used. The weights σ_k with which different multiple scattering amplitudes combine in the multiple scattering DPM can be calculated using the eikonal model. The weights σ_k are proportional to the probability of observing k inelastic collisions at given collision energy $\sqrt{s}$ and are written as [39,43,44]

$$\sigma_k(\xi) = \frac{\sigma_P}{kZ}\left[1 - e^{-Z}\sum_{i=0}^{k-1}\frac{Z^i}{i!}\right], \qquad k \geq 1, \tag{1}$$

where $\xi = \ln(\frac{s}{s_0})$, with $s_0 = 1$ GeV^2, $\sigma_P = 8\pi\gamma_P e^{\Delta\xi}$, and $Z = \frac{2C_E\gamma_P e^{\Delta\xi}}{R^2+\alpha'_P\xi}$. Here, σ_P is the Born term given by Pomeron exchange with intercept $\alpha_P(0) = 1 + \Delta$. The values of other parameters are given below and are taken from [39]: $R^2 = 3.3$ GeV^{-2}, $\gamma_P = 0.85$ GeV^{-2}, $C_E = 1.8$, $\Delta = 0.19$, $\alpha'_P = 0.25$ GeV^{-2}.

One of the most important parameters in Eq. (1) is Δ appearing in the Pomeron intercept, which is taken to be 0.19 and is motivated from the studies done on the LHC pp data in Ref. [39] and $\gamma^* p$ data in Ref. [45]. The rise in the single particle inclusive cross section per unit pseudorapidity with energy is governed by Δ. Parameters R and α'_P control the t dependence of the elastic peak [44,46]. The parameter γ_P is determined from the absolute normalization of the total ND inelastic cross section. A higher value of $C_E = 1.8$ [8] is needed to include the high-mass diffraction states. In the RFT, the large-mass diffraction states correspond to the triple-Pomeron graphs and to the loop graphs [8,39,45]. A smaller value of $C_E = 1.5$ is taken in Refs. [43,44] corresponding to 50% contribution of small-mass diffraction states relative to elastic contribution. The higher value of $C_E = 1.8$ takes care of the triple-Pomeron graphs from the high-mass diffraction states at the LHC energies. It is to be noted that the increase in the contribution of the high-mass diffraction states increases by 6% with an increase in center-of-mass-energy from 2.76 to 14 TeV.

From the Abramovskii, Gribov and Kancheli cancellation [47], one writes

$$\sigma_P(\xi) = \sum_{k\geq 1} k\sigma_k(\xi). \tag{2}$$

The nondiffractive inelastic scattering cross section σ_{ND}^{pp} can be obtained from the weights σ_k as

$$\sigma_{ND}^{pp} = \sum_{k\geq 1} \sigma_k(\xi). \tag{3}$$

The ends of each chain are linked to the valence or sea quarks of the colliding hadrons. The energy flow within the chains is governed by the parton distribution functions of the quarks in the colliding hadrons. For computing the hadronic spectra in the inelastic collision, the fragmentation functions are required. However, for the central rapidity region, the average hadronic multiplicities can be computed without using the fragmentation functions but using the rapidity position of each chain.

If we know the number of $2k$ chains in the k inelastic scatterings with the σ_k combining cross section, the underlying mechanism of the particle production can be predicted. The average number of inelastic collisions is denoted by $\langle k \rangle$ and is calculated as

$$\langle k \rangle = \frac{\sum_{k\geq 1} k\sigma_k(\xi)}{\sum_{k\geq 1}\sigma_k(\xi)} = \frac{\sigma_P(\xi)}{\sigma_{ND}^{pp}}. \tag{4}$$

Small clusters of hadrons are produced as a result of fragmentation of chains in the inelastic scatterings. In the DPM, the clusters produced in different chains are assumed to be uncorrelated [8]. Any cluster would contain on an average K number of charged particles. A value of $K = 1.4$ is taken as it is found to describe well the hadronic spectra in pp collisions [48,49]. The probability of discovering n_c clusters of hadrons in k inelastic collisions is assumed to be given by the Poisson distribution [38]

$$P_{n_c}^k = e^{-k\langle n_c\rangle_0} \frac{(k\langle n_c\rangle_0)^{n_c}}{n_c!}. \tag{5}$$

Here, $\langle n_c \rangle_0$ is the mean cluster multiplicity in a single inelastic scattering, and it is related to the corresponding mean charged particle multiplicity $\langle n \rangle_0$, as $\langle n_c \rangle_0 = \langle n \rangle_0 / K$.

The value of $\langle n \rangle_0$ in a given central pseudorapidity region can be obtained by integrating the charged multiplicity per unit pseudorapidity in an individual scattering, $\frac{dN_0^{pp}}{d\eta}$, as shown below:

$$\langle n \rangle_0 = \int_{\eta-\eta_0}^{\eta+\eta_0} \frac{dN_0^{pp}}{d\eta} d\eta \sim 2\eta_0 \frac{dN_0^{pp}}{d\eta}(\eta^* = 0) = 3\eta_0. \tag{6}$$

The quantity $\frac{dN_0^{pp}}{d\eta}(\eta^* = 0) = 1.5$ is independent of the collision energy at midrapidity and at high energy as described in Ref. [39]. Using $\langle k \rangle$, the value of differential charged multiplicity in a given psuedorapidity interval is calculated as

$$\frac{dN^{pp}}{d\eta} = \langle k \rangle \frac{dN_0^{pp}}{d\eta}. \tag{7}$$

The total cluster multiplicity is then given by the equation

$$P_{n_c} = \frac{\sum_{k\geq 1}\sigma_k P_{n_c}^k}{\sigma_{ND}^{pp}}. \tag{8}$$

The shape of the probability distributions and the KNO scaling violations due to the rise in the high-multiplicity tail can be explained in the framework of the DPM [8–10]. This is attributed to the increase in the contribution from the multichain graphs with the increase in center-of-mass energies, and it affects the high-multiplicity region. One of the established results from the DPM is the broadening of the multiplicity distribution in the limited pseudorapidity intervals, due to increase in the relative effect of multichains. However, in smaller pseudorapidity intervals, the short-range correlations dominate, and multiplicity distributions become narrower.

The values of $\frac{dN^{pp}}{d\eta}$, σ_{ND}^{pp}, and $\sigma_{\rm tot}^{pp}$ from the DPM at various collision energies reported in Ref. [39] are reproduced as shown in the Table I. Their values at the collision energies of 13, 13.6 (ongoing RUN3), and future LHC collision energy of 27 TeV are also calculated and shown in the given table.

III. KNO FORMALISM

The KNO form of the multiplicity distributions is written in terms of $\Psi(z)$,

$$\Psi(z) = \langle n \rangle P_n = \langle n_c \rangle P_{n_c}, \tag{9}$$

where

$$z = n/\langle n \rangle = n_c/\langle n_c \rangle. \tag{10}$$

Here, n is the number of emitted charged particles, and $\langle n \rangle$ is its mean value. The latter can be calculated from the average cluster multiplicity using the equation

TABLE I. Cross sections of total and nondiffractive processes for pp interactions and the charged particle pseudorapidity densities in the central rapidity region corresponding to $\sqrt{s}$.

$\sqrt{s}$ (GeV)	$\frac{dN^{pp}}{d\eta}$ $(y^* = 0)$	σ_{ND}^{pp}	$\sigma_{\rm tot}^{pp}$
200	2.99	31.22	41.62
540	3.50	38.97	54.39
900	3.82	43.33	61.85
1800	4.34	49.64	72.93
2360	4.57	52.24	77.54
2760	4.71	53.77	80.27
7000	5.70	63.33	97.57
13000	6.50	70.15	110.03
13600	6.57	70.66	110.96
27000	7.66	78.67	125.68

$\langle n\rangle = \langle k\rangle\langle n\rangle_0 = 3\eta_0\langle k\rangle$. The relation between n and n_c is given by using $n_c = n/K$, also $\langle n_c\rangle = \langle n\rangle/K$.

IV. DATA ANALYZED

The charged hadron multiplicity in NSD processes in pp collisions has been measured by the CMS Collaboration [42] at various center-of-mass energies, $\sqrt{s} = 0.9$, 2.36, and 7 TeV in restricted pseudorapidity intervals of $|\eta| < 0.5$ and $|\eta| < 2.4$. These experimental results are available on HEPData [50] and have been used for the present study. In addition, for detailed comparison, we used the Monte Carlo (MC) event generator PYTHIA8.306 for the generation of 10^7 pp NSD events at each $\sqrt{s}$ and in each pseudorapidity interval under study.

With the aim of providing a better description of the observables of the data, event generators have adjustable parameters to control the behavior of the event modeling. These observables may be sensitive to partons from initial-state radiation and final-state radiation, underlying events consisting of beam remnants, particles produced in multiple-parton interaction (MPI), etc. The processes of hadronization and MPI are particularly afflicted, as they involve nonperturbative QCD physics. A good modeling of hadronization is required. The interaction of partons just before hadronizing is modeled by color reconnection. A set of parameters, which need to be adjusted to fit some aspects of the data, is referred to as a tune. The experimental data from an experiment is often fitted to the predictions from an event generator by tuning and optimizing these parameters.

Description of PYTHIA as an event generator can be found in Ref. [51]. For the present analysis, PYTHIA8 tunes, Monash [52] and 4C [53], are used for studying the charged hadron multiplicity distributions. The MDs have also been simulated for $\sqrt{s} = 13$, 13.6, and 27 TeV using PYTHIA8.3 for comparison with the model and for predicting the multiplicity at the future LHC energy of 27 TeV. Both tunes have strong color reconnection implemented, which results in reduction of charged particles in the final state. The MPI, on the other hand, increases the charged multiplicity.

Other nonperturbative processes in terms of string interactions called string shoving [54,55] and rope hadronization [56] have been studied using PYTHIA8 [57–60]. These processes have been able to explain the QGP like signals in the pp collisions since they were first discovered at the LHC in 2010. The first implementation of the rope hadronization model in the event generators was done in DIPSY [57]. It is a collective effect which results from the overlapping of closely spaced strings forming a wider color flux tube called a rope. Each string would hadronize separately but not independently as the string tension is modified. This results in the strangeness enhancement in pp collisions for the high-multiplicity events. However, a very minor correction in the total multiplicity of the event is expected due to these effects as explained in Ref. [57].

V. RESULTS

A. Multiplicity distributions

For a probability P_n of producing n charged particles, the mean charged multiplicity is defined as

$$\langle n\rangle = \frac{\sum nP_n}{\sum P_n}. \tag{11}$$

Figure 1 shows the charged hadron multiplicity distributions for $\sqrt{s} = 0.9$, 2.36, and 7 TeV in the pseudorapidity $|\eta| < 0.5$ interval. The data obtained by the CMS Collaboration are shown and compared with the distributions simulated by using PYTHIA8 for two different tunes, Monash and 4C. In each plot, the lower panel shows the ratio of data versus MC tunes. It is observed that the charged MDs agree with the experimental distributions in general, with small fluctuations at higher-multiplicity tails as can be observed from the ratio plots, at each energy.

Figure 2 shows the charged hadron multiplicity distributions for $\sqrt{s} = 0.9$, 2.36, and 7 TeV in the pseudorapidity interval $|\eta| < 2.4$. Again, the data obtained by the CMS Collaboration are shown and compared with the distributions simulated by using PYTHIA8 for two different tunes, Monash and 4C. The multiplicity distributions have different shapes in the two pseudorapidity intervals. A shoulder structure in the low-multiplicity region in $|\eta| < 2.4$ interval can be clearly seen for all energies.

It is observed that the ratio of the experimental MDs to the simulated data fluctuates around ~1. However, there is an observable deviation at mid-and-higher multiplicities. In the mid-multiplicity region, PYTHIA8 underestimates the MDs, and in the higher-multiplicity region, it overestimates. This effect gets pronounced with an increase in the center-of-mass energy as shown in the ratio plots. Both Monash and 4C tunes show similar behavior at all energies.

B. Mean multiplicity from DPM and PYTHIA

Table II presents the mean multiplicity at different center-of-mass energies for the CMS data [42], for DPM described in Sec. II and for PYTHIA8 tunes, Monash and 4C, in the $|\eta| < 2.4$ interval. It is observed that values from the DPM and those from PYTHIA8 agree with the experimental values within the error limits. However, the model tends to underestimate the experimental mean multiplicity, while both tunes of PYTHIA slightly overestimate. Figure 3 shows the variation of mean multiplicity $\langle n\rangle$ with $\sqrt{s}$ from 0.9 to 27 TeV. Data from the CMS experiment are shown in comparison to the model and MC simulations from PYTHIA for the tunes Monash and 4C. The variation in each case can be represented by a fit of the type

$$\langle n\rangle = a + b\ln\sqrt{s} + c(\ln\sqrt{s})^2. \tag{12}$$

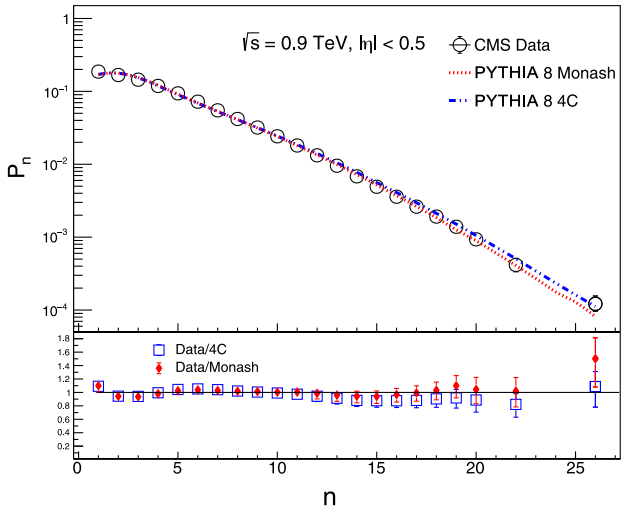

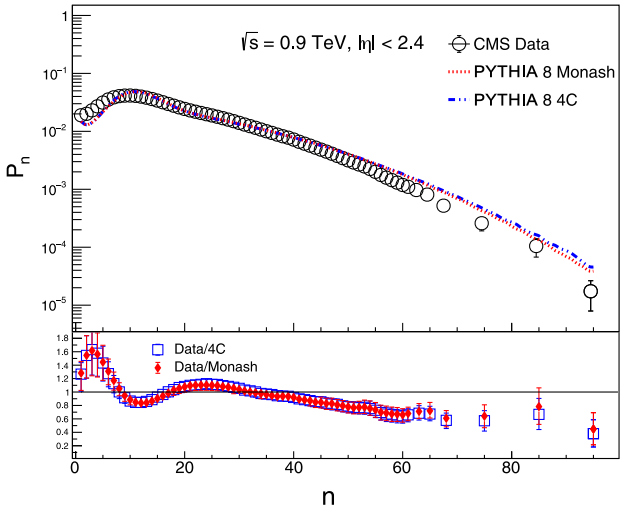

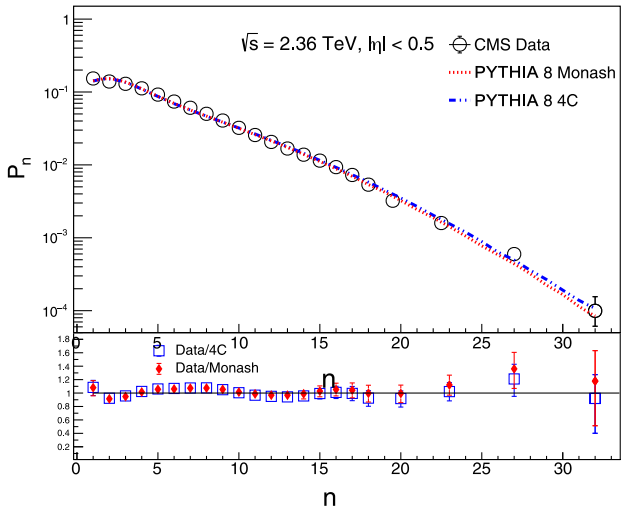

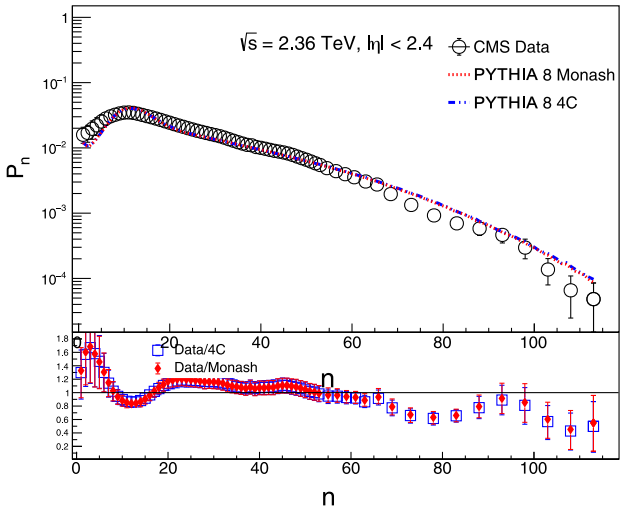

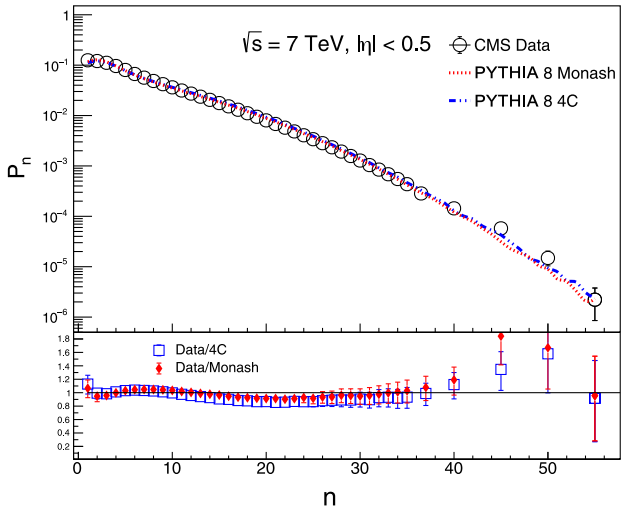

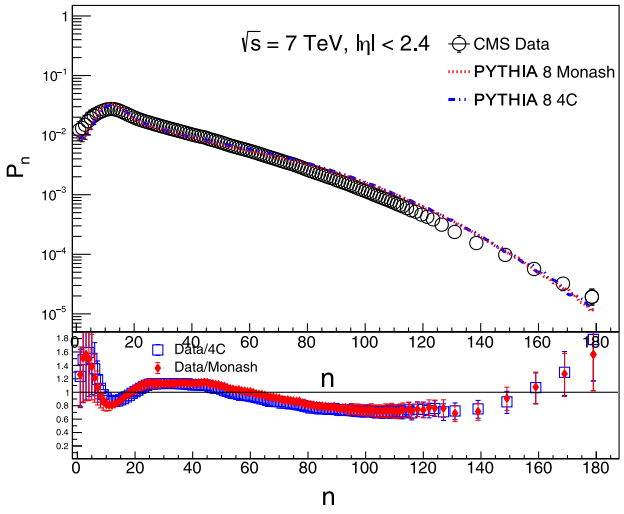

FIG. 1. Charged hadron multiplicity distributions for $\sqrt{s} = 0.9$, 2.36, and 7 TeV in the pseudorapidity $|\eta| < 0.5$. Points represent the data obtained by the CMS Collaboration, and the lines represent the values from PYTHIA for two tunes. In each plot, the lower panel shows the ratio of data versus MC tunes.

FIG. 2. Charged hadron multiplicity distributions for $\sqrt{s} = 0.9$, 2.36, and 7 TeV in the pseudorapidity $|\eta| < 2.4$ interval. Points represent the data obtained by the CMS Collaboration, and the lines represent from PYTHIA for Monash and 4C tunes. In each plot, the lower panel shows the ratio of data versus MC tunes.

TABLE II. $\langle n \rangle$ as a function of $\sqrt{s}$ for $|\eta| < 2.4$. For each $\sqrt{s}$, a sample of 10 million events is simulated for every $\langle n \rangle$. Thus, the statistical errors are negligible and hence have not been quoted. Values shown with $(*)$ are predicted from (12).

$\sqrt{s}$ (TeV)	Experiment [42]	Model	4C	Monash
0.9	$17.9 \pm 0.1^{+1.1}_{-1.1}$	18.33	19.68	19.65
2.36	$22.9 \pm 0.5^{+1.6}_{-1.5}$	21.93	24.71	24.55
7	$30.4 \pm 0.2^{+2.2}_{-2.0}$	27.35	33.22	32.29
13	$35.60^{(*)}$	31.23	39.67	37.85
13.6	$36.00^{(*)}$	31.55	40.17	38.24
27	$42.52^{(*)}$	36.77	49.00	45.51

For the CMS data, the fit parameters are given by $a = 26.70 \pm 2.63$, $b = -13.94 \pm 0.76$, and $c = 3.34 \pm 0.16$. An extrapolation of the fit to higher $\sqrt{s}$ predicts the $\langle n \rangle$ as shown in the Table II. The 68.3% confidence interval (CI) (1σ) band on the fit function is shown in Fig. 3 along with the prediction for experimental $\langle n \rangle$ at 13, 13.6, and 27 TeV. The values at these higher energies from the DPM and two PYTHIA tunes lie within the 68.3% CI band.

C. KNO multiplicity distributions

The KNO multiplicity distributions in $\Psi(z)$ versus z are presented in Figs. 4 and 5 for various center-of-mass energies in $|\eta| < 0.5$ and $|\eta| < 2.4$ intervals, respectively. The experimental data [50] are compared with predictions from the DPM and with the MC data simulated from PYTHIA for the tunes, Monash and 4C. For $|\eta| < 0.5$, it is observed that the PYTHIA tunes agree with the data at lower z but show increasing disagreement above $z \sim 4$ at all energies. The deviation of the KNO distributions from the DPM starts at $z \sim 6$ for $|\eta| < 0.5$ at all energies. For the $|\eta| < 2.4$ interval, the agreement with both PYTHIA tunes is

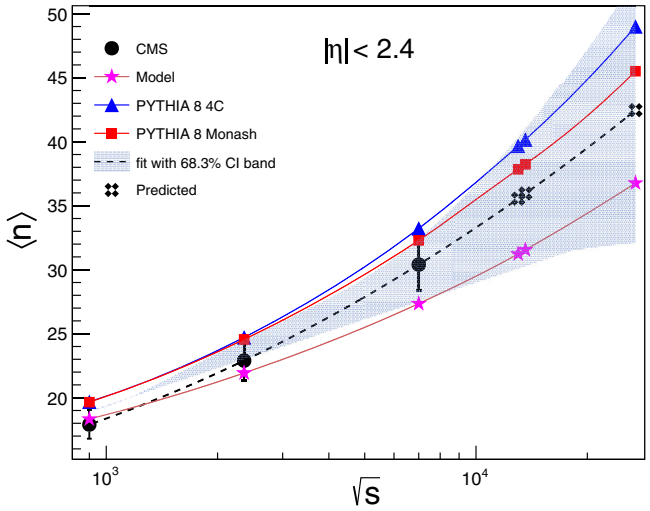

FIG. 3. Mean multiplicity $\langle n \rangle$ as a function of $\sqrt{s}$ for $|\eta| < 2.4$.

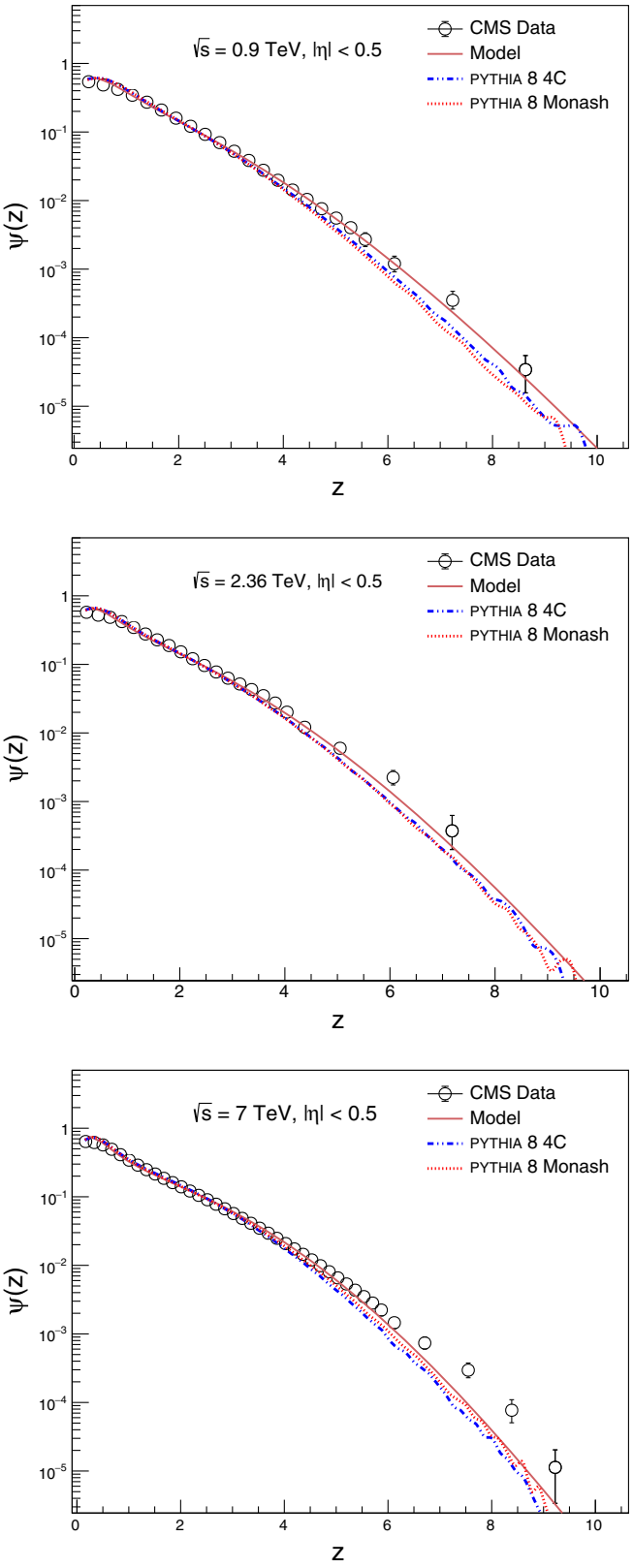

FIG. 4. KNO distributions at $\sqrt{s} = 0.9$, 2.36, and 7 TeV in the pseudorapidity $|\eta| < 0.5$. Points represent the data obtained by the CMS experiment, solid lines represent the predictions from the model, and dotted lines represent the distributions generated from PYTHIA for two different tunes.

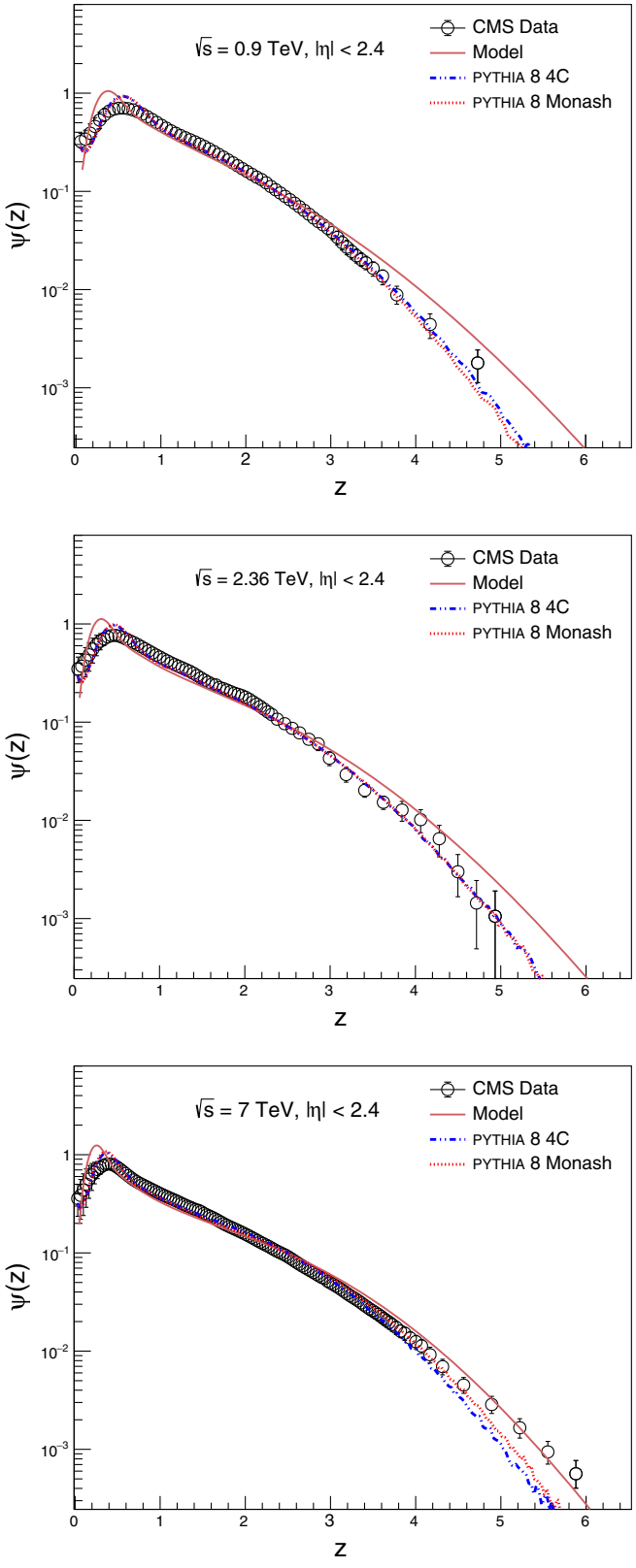

FIG. 5. KNO distributions at $\sqrt{s} = 0.9$, 2.36, and 7 TeV in the pseudorapidity $|\eta| < 2.4$. Points represent the data obtained by the CMS experiment, solid lines represent the predictions from the model, and dotted lines represent the distributions generated from PYTHIA for two different tunes.

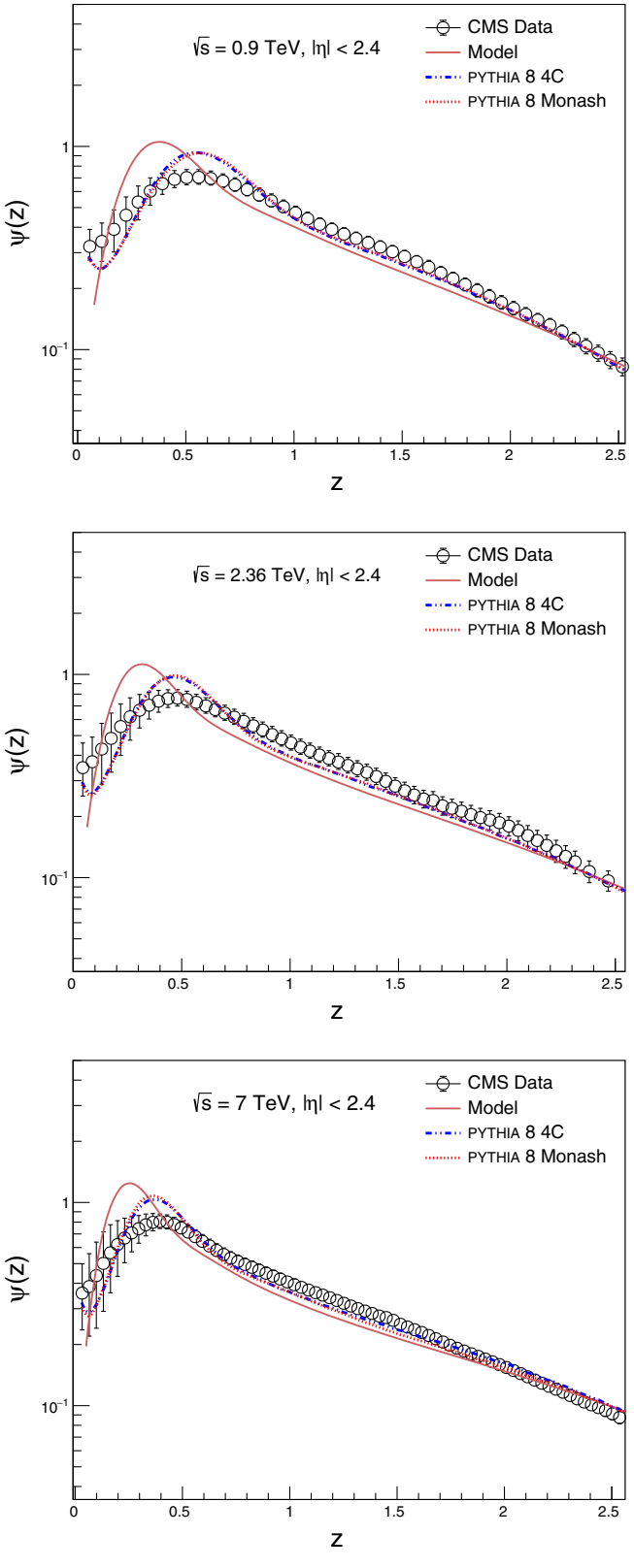

FIG. 6. KNO distributions in the range $z = 0$ to 2.5 for different center-of-mass energies, in the pseudorapidity interval $|\eta| < 2.4$. Solid lines represent the predictions from the model, and dotted lines represent the distributions generated from PYTHIA for two different tunes at each energy.

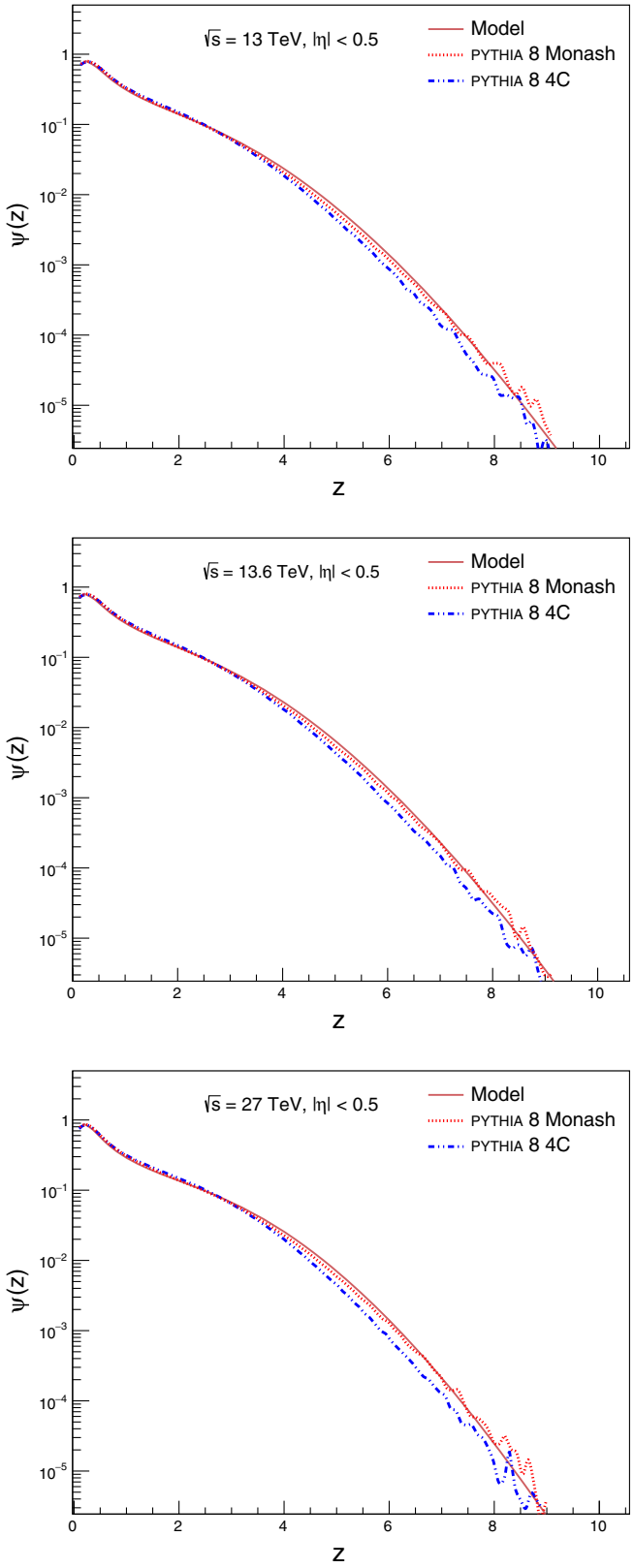

FIG. 7. KNO distributions at $\sqrt{s} = 13$, 13.6, and 27 TeV in the pseudorapidity interval $|\eta| < 0.5$. Solid lines represent the predictions from the model, and dotted lines represent the distributions generated from PYTHIA for two different tunes at each energy.

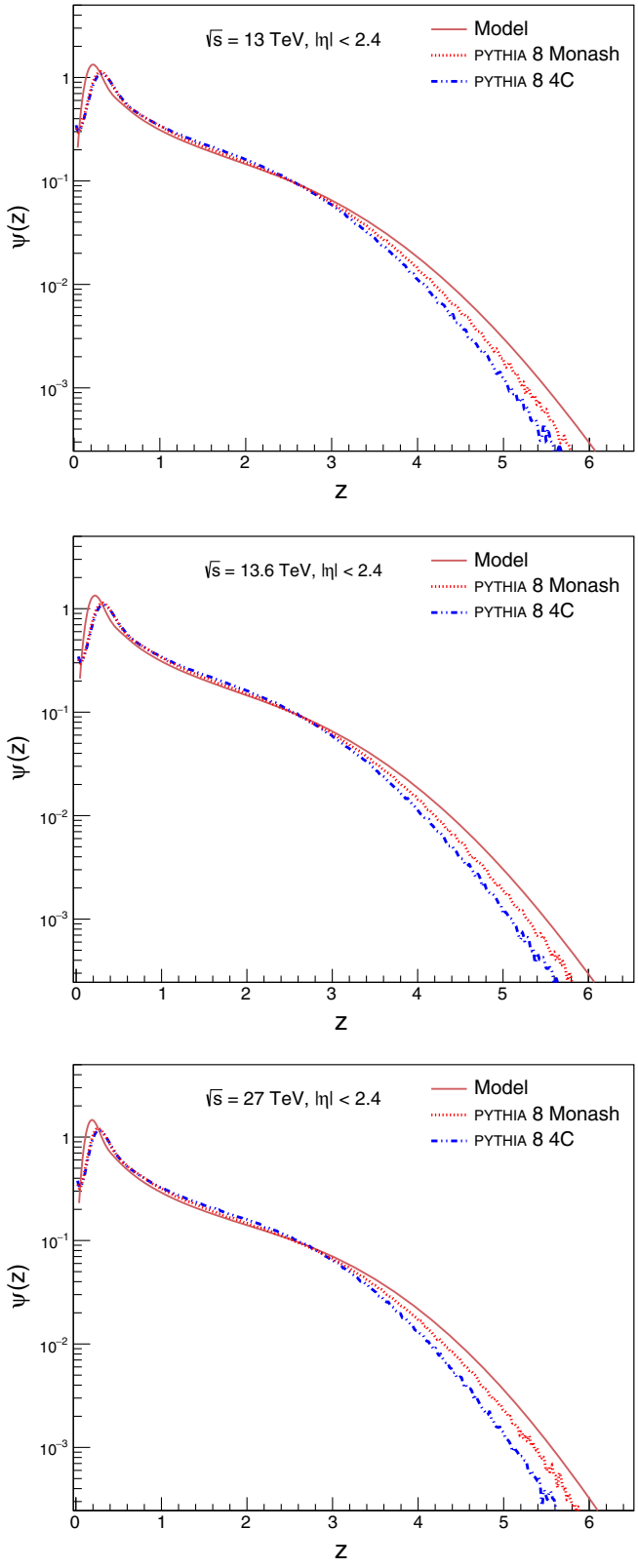

FIG. 8. KNO distributions at $\sqrt{s} = 13$, 13.6, and 27 TeV in the pseudorapidity interval $|\eta| < 2.4$. Solid lines represent the predictions from the model, and dotted lines represent the distributions generated from PYTHIA for two different tunes at each energy.

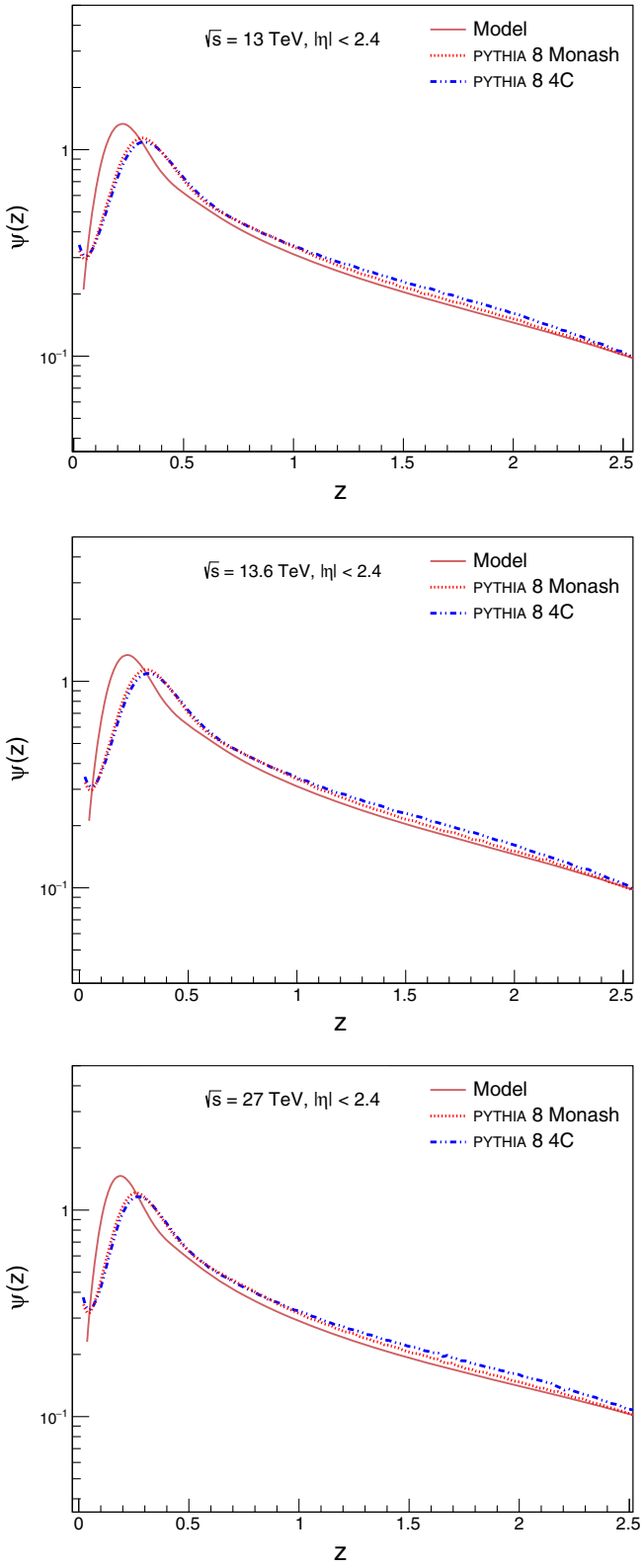

FIG. 9. KNO distributions in the range $z = 0$ to 2.5 for $\sqrt{s} =$ 13.6 and 27 TeV, in the pseudorapidity interval $|\eta| < 2.4$. Solid lines represent the predictions from the model, and dotted lines represent the distributions generated from PYTHIA for two different tunes at each energy.

better as seen in Fig. 5, and the deviation is observed only at 7 TeV for $z > 4$. However, in this region, the model deviates from the data at all $\sqrt{s}$ for $z > 3$.

A shoulder structure is observed for each distribution in the $|\eta| < 2.4$ region. The model is not able to describe the shoulder structure fully for all energies. The data when compared with MC distributions from PYTHIA show an agreement better than the model, and the agreement improves with the increasing collision energy. For a better comparison, a blown-out view of every distribution in the region around the peak is presented for the higher pseudorapidity region.

The authors in Refs. [61–63] show that the KNO scaling violation in PYTHIA is due to color reconnection and MPIs. The MPIs become more prominent at higher collider energies, and it can increase the average multiplicity three times, which makes the KNO distribution wider, whereas the color reconnection, which models the interaction between color fields just before hadronization, can decrease the charged multiplicity by 30%. It results in a narrower KNO distribution.

Figure 6 shows the KNO distributions around the peak values for $z < 2.5$ at $\sqrt{s} = 0.9$, 2.36, and 7 TeV in the $|\eta| < 2.4$ range. It is observed that there is a disagreement between the model predictions and the data. Though the shoulder structure present in the data is reproduced by the model, the position of the peak is shifted to the lower multiplicities in comparison to the data. The MC and the data distributions are peaked nearly at the same positions. The distributions from the tunes Monash and 4C agree closely with each other and also with the data within the limits of experimental errors.

The predictions for the KNO distributions from the DPM and PYTHIA8 tunes are presented for the RUN2, RUN3, and future LHC energies at $\sqrt{s} = 13$, 13.6, and 27 TeV in Figs. 7 and 8 for the $|\eta| < 0.5$ and $|\eta| < 2.4$ intervals, respectively. Also, Fig. 9 shows the KNO distributions around the peak values with $z < 2.5$ at these energies in the $|\eta| < 2.4$ range.

It is also observed that the peak shifts toward a smaller z value as the collision energy increases from 0.9 to 27 TeV. In the $|\eta| < 0.5$ region, the predictions from DPM and PYTHIA8 tunes agree, although the PYTHIA Monash tune is closer to the model. For $|\eta| < 2.4$, the two tunes of PYTHIA agree closely; however, the distribution from the DPM is shifted at each energy. Below $z < 2.5$, the model underestimates the PYTHIA8 predictions; however, above ~2.5, the model overestimates the PYTHIA8 predictions. Similar observations are made from Fig. 9 showing the distributions around the peak.

VI. CONCLUSION

A detailed analysis and comparison of the charged hadron multiplicities in pp collisions at various center-of-mass

energies at the LHC is presented. The analysis uses the data classified as nonsingle diffractive events obtained by the CMS experiment at $\sqrt{s} = 0.9$, 2.36, and 7 TeV in the two pseudorapidity intervals, $|\eta| < 0.5$ and $|\eta| < 2.4$. These data are compared with predictions of the dual parton model and MC simulations of charged hadron production by using two different tunes of event generator PYTHIA8. Out of the two tunes used, Monash is the default tune in PYTHIA, and 4C is the tune used by the CMS experiment. Using these tunes and calculations from the model, multiplicities are also obtained at $\sqrt{s} = 13$, 13.6, and 27 TeV. The LHC RUN3 has just started taking data at 13.6 TeV. This analysis presents predictions for the charged hadron multiplicities at these energies and also for the future LHC energy of 27 TeV.

It is observed that the MDs in the $|\eta| < 0.5$ interval agree with the experimental distributions at $\sqrt{s} = 0.9$, 2.36, and 7 TeV. For the $|\eta| < 2.4$ interval, PYTHIA8 predictions underestimate the experimental MDs in the mid-multiplicity region for both Monash and 4C tunes, as seen in the ratio plot. For the higher-multiplicity region, PYTHIA8 predictions overestimate the experimental MDs. In addition, a shoulder structure can be observed in the lowest-multiplicity region.

The mean multiplicities obtained from the data, model, and MC are in good agreement for $\sqrt{s} = 0.9$ and 2.36 TeV. The mean multiplicity from the model soon starts to deviate from MC and the data at higher energy. The $\langle n \rangle$ of the data and MC are in agreement within the error limit of experimental data at $\sqrt{s} = 7$ TeV. However, the model systematically underestimates the experimental values from the CMS data, and PYTHIA overestimates. The deviation of the mean from the model gets more pronounced at center-of-mass energy beyond 7 TeV.

KNO distributions obtained from the data [42], model, and MC are presented for $\sqrt{s} = 0.9$, 2.36, and 7 TeV in Figs. 7 and 8. For $|\eta| < 0.5$, distributions from the model are found to deviate from the data at $z \sim 6$, while for MC distributions, the deviation is seen much earlier at $z \sim 4$. Similarly, the KNO distributions at these energies in the $|\eta| < 2.4$ interval show deviation of distributions from the model and the data at $z \sim 3$, and for MC distributions, the deviation from the data starts at $z \sim 4$. Exceptionally, the distribution from the model at $\sqrt{s} = 7$ TeV follows the data very closely, while the MC distributions show deviation.

It may be observed that at nearly the same values of z the increase with energy of the high-multiplicity tail of the KNO curve is larger for the rapidity region $|\eta| < 2.4$ than for $|\eta| < 0.5$. In the DPM, the mechanism of particle production in hadron-hadron collisions comes from the weighted superposition of chains, each of which results from $q - \bar{q}$ color separation. An important result from DPM [9,10] explains that the multiplicity distributions are broader in the central rapidity intervals of limited length, as in this case the relative effect of multichains increases. However, for the smaller rapidity intervals, the short-range correlations within the individual chains dominate, leading to the narrower multiplicity distributions.

There are MC event generators which are based on DPM and QGSM. PHOJET [64,65] and DPMJET [66] based on the DPM are used for studying pp, p-nucleus, and nucleus-nucleus collisions. The MC generator QGSJET [67] uses the QGSM for describing hadronic and nuclear collision data. A detailed comparison of the NSD charged particle multiplicity for the LHC energies using different model predictions, including PYTHIA8, PHOJET, DPMJET, and QGSJET, can be found in Refs. [57,68,69]. It is also concluded in these papers that the RFT-based MC generators are able to reproduce the NSD charged multiplicity KNO distributions but miss the intricate details especially at the higher LHC energies. The peak at lower-multiplicity is reported as shifted toward lower n, and the distribution has a much longer tail.

The data from the CMS are not available for analysis at $\sqrt{s} = 13$ TeV, for the NSD events in the same transverse momentum range. The LHC RUN3 has started very recently, and the data at the collision energy of 13.6 TeV is being collected by the experiments at the LHC.

We present the predictions for the mean multiplicities and the multiplicity distributions as estimated from the model and PYTHIA8 for the two tunes for these energies. Mean multiplicity and the KNO distributions for the future LHC energy of 27 TeV are also predicted.

It is also observed that the KNO distributions obtained from the two tunes agree very closely, though the low-z region below the peak shows disagreement between the model and the data. The peak of the KNO distribution in each case shifts toward smaller z value as the collision energy increases from 0.9 to 27 TeV.

The observations from the present study are indicative of the trends in the future data from the LHC. Comparison with the data when they become available makes an interesting study and may lead to a new direction in our current understanding.

[1] Z. Koba, H. B. Nielsen, and P. Olesen, Nucl. Phys. **B40**, 317 (1972).
[2] G. Arnison, A. Astbury *et al.* (UA1 Collaboration), Phys. Lett. **123B**, 108 (1983).
[3] G. J. Alner, K. Åsman *et al.* (UA5 Collaboration), Phys. Lett. **167B**, 476 (1986).
[4] R. E. Ansorge, B. Åsman *et al.* (UA5 Collaboration), Z. Phys. C **43**, 357 (1989).

[5] P. Abreu, W. Adam *et al.* (DELPHI Collaboration), Z. Phys. C **50**, 185 (1990).
[6] D. Buskulic, D. Casper *et al.* (ALEPH Collaboration), Z. Phys. C **69**, 15 (1995).
[7] A. Capella, U. Sukhatme, C.-I. Tan, and J. T. T. Van, Phys. Lett. **81B**, 68 (1979).
[8] A. Capella, U. Sukhatme, C.-I. Tan, and J. T. T. Van, Phys. Rep. **236**, 225 (1994).
[9] A. Capella and J. Tran Thanh Van, Z. Phys. C **23**, 165 (1984).
[10] A. Capella, A. Staar, and J. T. T. Van, Phys. Rev. D **32**, 2933 (1985).
[11] A. Capella and J. Tran Thanh Van, Z. Phys. C **18**, 85 (1983).
[12] A. Kaidalov, Phys. Lett. **116B**, 459 (1982).
[13] A. Kaidalov and K. Ter-Martirosyan, Phys. Lett. **117B**, 247 (1982).
[14] V. Gribov, Zh. Eksp. Teor. Fiz. **53**, 654 (1967).
[15] C. Hong-Mo, J. E. Paton, T. S. Tsun, and N. S. Wai, Nucl. Phys. **B92**, 13 (1975).
[16] G. F. Chew and C. Rosenzweig, Nucl. Phys. **B104**, 290 (1976).
[17] G. F. Chew and C. Rosenzweig, Phys. Rep. **41**, 263 (1978).
[18] G. F. Chew, D. Issler, B. Nicolescu, and V. Poenaru, in *19th Rencontres de Moriond: New Particle Production at High-Energy (Hadronic Session)* (La Plagne, France, 1984), p. 143.
[19] C. Hong-Mo and T. S. Tsun, Nucl. Phys. **B118**, 413 (1977).
[20] A. Capella and J. Tran Than Van, Z. Phys. C **10**, 249 (1981).
[21] A. Capella, C. Pajares, and A. Ramallo, Nucl. Phys. **B241**, 75 (1984).
[22] C. Wei-Qin, C. B. Chiu, H. Zuoxiu, and D. M. Tow, Phys. Rev. Lett. **44**, 518 (1980).
[23] C. Pajares and A. Ramallo, Phys. Lett. **107B**, 373 (1981).
[24] A. Capella, J. Kwieciński, and J. T. T. Van, Phys. Lett. **108B**, 347 (1982).
[25] W. Chao and H. Pirner, Z. Phys. C **14**, 165 (1982).
[26] V. Khachatryan *et al.* (CMS Collaboration), J. High Energy Phys. 09 (2010) 091.
[27] V. Khachatryan *et al.* (CMS Collaboration), Phys. Rev. Lett. **116**, 172302 (2016).
[28] G. Aad *et al.* (ATLAS Collaboration), Phys. Rev. Lett. **116**, 172301 (2016).
[29] J. Adams *et al.* (STAR Collaboration), Phys. Rev. Lett. **95**, 152301 (2005).
[30] S. Chatrchyan *et al.* (CMS Collaboration), J. High Energy Phys. 07 (2011) 076.
[31] K. Werner, I. Karpenko, and T. Pierog, Phys. Rev. Lett. **106**, 122004 (2011).
[32] K. Dusling and R. Venugopalan, Phys. Rev. Lett. **108**, 262001 (2012).
[33] A. Dumitru, K. Dusling, F. Gelis, J. Jalilian-Marian, T. Lappi, and R. Venugopalan, Phys. Lett. B **697**, 21 (2011).
[34] M.-A. Sanchis-Lozano and E. Sarkisyan-Grinbaum, Phys. Lett. B **766**, 170 (2017).
[35] M.-A. Sanchis-Lozano and E. Sarkisyan-Grinbaum, Phys. Rev. D **96**, 074012 (2017).
[36] C. Andrés, A. Moscoso, and C. Pajares, Phys. Rev. C **90**, 054902 (2014).
[37] M. Braun, C. Pajares, and V. Vechernin, Eur. Phys. J. A **51**, 44 (2015).
[38] A. Capella and E. Ferreiro, arXiv:1301.3339.
[39] A. Capella and E. Ferreiro, Eur. Phys. J. C **72**, 1936 (2012).
[40] K. Aamodt *et al.* (ALICE Collaboration), Eur. Phys. J. C **68**, 89 (2010).
[41] V. Khachatryan *et al.* (CMS Collaboration), J. High Energy Phys. 02 (2010) 041.
[42] V. Khachatryan *et al.* (CMS Collaboration), J. High Energy Phys. 01 (2011) 079.
[43] K. Ter-Martirosyan, Phys. Lett. **44B**, 377 (1973).
[44] A. B. Kaidalov, Surv. High Energy Phys. **13**, 265 (1999).
[45] A. Capella, E. Ferreiro, C. Salgado, and A. Kaidalov, Nucl. Phys. **B593**, 336 (2001).
[46] S. Chatrchyan *et al.* (CMS Collaboration), J. High Energy Phys. 08 (2011) 141.
[47] V. Abramovsky, V. Gribov, and O. Kancheli, Yad. Fiz. **18**, 595 (1973).
[48] A. Capella and A. Ramallo, Phys. Rev. D **37**, 1763 (1988).
[49] K. Blöckman, *Proceedings of the International Symposium on Physics in Collision, Como, Italy* (Autun, France, 1985).
[50] E. Maguire, L. Heinrich, and G. Watt, J. Phys. Conf. Ser. **898**, 102006 (2017).
[51] C. Bierlich, S. Chakraborty *et al.*, arXiv:2203.11601.
[52] P. Skands, S. Carrazza, and J. Rojo, Eur. Phys. J. C **74**, 3024 (2014).
[53] R. Corke and T. Sjöstrand, J. High Energy Phys. 03 (2011) 032.
[54] C. Bierlich, G. Gustafson, and L. Lönnblad, Phys. Lett. B **779**, 58 (2018).
[55] C. Bierlich, S. Chakraborty, G. Gustafson, and L. Lönnblad, J. High Energy Phys. 03 (2021) 270.
[56] C. Bierlich, G. Gustafson, and L. Lönnblad, arXiv:1612.05132.
[57] C. Bierlich, G. Gustafson, L. Lönnblad, and A. Tarasov, J. High Energy Phys. 03 (2015) 148.
[58] S. Chakraborty, *Proc. Sci.*, HardProbes2020 (2021) 134.
[59] P. Chakraborty and S. Dash, Phys. Rev. C **102**, 055202 (2020).
[60] S. Chakraborty, SciPost Phys. Proc. **10**, 017 (2022).
[61] M. A. Mahmoud, Particles **5**, 96 (2022).
[62] R. Vértesi, A. Gémes, and G. G. Barnaföldi, Phys. Rev. D **103**, L051503 (2021).
[63] A. Ortiz and L. V. Palomo, Phys. Rev. D **99**, 034027 (2019).
[64] R. Engel, Z. Phys. C **66**, 203 (1995).
[65] R. Engel and J. Ranft, Phys. Rev. D **54**, 4244 (1996).
[66] S. Roesler, R. Engel, and J. Ranft, in *Advanced Monte Carlo for Radiation Physics, Particle Transport Simulation and Applications* (Springer Berlin Heidelberg, Berlin, Heidelberg, 2001), pp. 1033–1038.
[67] N. Kalmykov, S. Ostapchenko, and A. Pavlov, Phys. At. Nucl. **58**, 1728 (1995), https://www.osti.gov/biblio/183734.
[68] D. d'Enterria, R. Engel, T. Pierog, S. Ostapchenko, and K. Werner, Astropart. Phys. **35**, 98 (2011).
[69] D. d'Enterria and T. Pierog, J. High Energy Phys. 08 (2016) 170.